Journal of Power Sources 375 (2018) 21–28

Contents lists available at ScienceDirect

Journal of Power Sources

journal homepage: www.elsevier.com/locate/jpowsour

Enhancing the electrochemical performance of Li-rich layered oxide $Li_{1.13}Ni_{0.3}Mn_{0.57}O_2$ via WO_3 doping and accompanying spontaneous surface phase formation

Jiajia Huang, Haodong Liu, Tao Hu, Ying Shirley Meng, Jian Luo*

Department of NanoEngineering, Program of Materials Science and Engineering, University of California, San Diego, La Jolla, CA 92093-0448, USA

HIGHLIGHTS

- WO_3 doping improves the $Li_{1.13}Ni_{0.3}Mn_{0.57}O_2$ performance via forming a surface phase.
- The surface phase forms spontaneously via a facile mixing and annealing route.
- The surface phase has distinct structure, composition, and valence state.
- The discharge capacity is increased by ~13% at C/20 and by ~200% at 40C.
- The spontaneously-formed surface phase also improves the cycling stability.

ARTICLE INFO

Keywords:
Lithium ion batteries
Li-excess layered oxide
High energy density cathode
Surface phase
Complexion

ABSTRACT

WO_3 doping and accompanying spontaneous formation of a surface phase can substantially improve the discharge capacity, rate capability, and cycling stability of Co-free Li-rich layered oxide $Li_{1.13}Ni_{0.3}Mn_{0.57}O_2$ cathode material. X-ray photoelectron spectroscopy, in conjunction with ion sputtering, shows that W segregates to the particle surfaces, decreases the surface Ni/Mn ratio, and changes the surface valence state. High-resolution transmission electron microscopy further suggests that W segregation increases surface structural disorder. The spontaneous and simultaneous changes in the surface structure, composition, and valence state represent the formation of a surface phase (complexion) as the preferred surface thermodynamic state. Consequently, the averaged discharge capacity is increased by ~13% from 251 to 284 mAh g^{-1} at a low rate of C/20 and by ~200% from 30 to 90 mAh g^{-1} at a high rate of 40C, in comparison with an undoped specimen processed under identical conditions. Moreover, after 100 cycles at a charge/discharge rate of 1C, the WO_3 doped specimen retained a discharge capacity of 188 mAh g^{-1}, being 27% higher than that of the undoped specimen. In a broader context, this work exemplifies an opportunity of utilizing spontaneously-formed surface phases as a scalable and cost-effective method to improve materials properties.

1. Introduction

Li- and Mn-rich layered oxides $xLi(Li_{1/3}Mn_{2/3})O_2{\cdot}(1\text{-}x)LiMO_2$ (that can alternatively be expressed as $xLi_2MnO_3{\cdot}(1\text{-}x)LiMO_2$) ($0 < x < 1$; M = Mn, Ni, Co) are promising candidates of next-generation cathode materials for lithium ion batteries due to their high specific capacity of > 280 mAh g^{-1}; with an average discharge voltage of ~3.6 V, this capacity corresponds to an energy density of > 1000 Wh kg^{-1} [1–3]. The Li-rich layered oxides are also low cost and environmentally friendly due to the reducing of Co content in their composition. However, the practical applications of these layered oxides are still hindered by the irreversible capacity loss in the first cycle, the subsequent poor cycling stability, the low rate capability, and the voltage fading [4–6].

It is interesting to note that the above-mentioned challenging electrochemical properties can be highly affected by the surface properties of the Li-rich layered oxides. The significant irreversible capacity loss in the first cycle is believed to be resulted from formation of oxygen vacancies [7,8] and/or the occupation of lithium sites by transition metal ions on the surfaces (when the cathode is charged over 4.4 V) [9], which subsequently triggers an irreversible surface phase-like transition from the layered structure to a spinel-like structure [1,9–11]. Moreover, the rate capability can also be explained by the above-mentioned surface structure/chemistry changes as the lithium diffusion path could be partially blocked by the occupancy of lithium layer sites by transition

* Corresponding author.
E-mail address: jluo@alum.mit.edu (J. Luo).

https://doi.org/10.1016/j.jpowsour.2017.11.048
Received 4 September 2017; Received in revised form 24 October 2017; Accepted 14 November 2017

metal cations [5,6,9,12–17]. Hence, surface modifications could be an effective way to improve electrochemical performance of Li-rich layered cathode materials. Here, we explore the possibility of utilizing WO_3 segregation induced formation of a surface phase (also known as "complexion" [18,19]) with structure and chemistry that are markedly different from those inside a bulk phase as a spontaneous surface modification method to improve the properties.

Recently, Sathiya et al. reported that Ru(4d) substitution of *M*(3d) in Li_2MO_3 in the bulk phase can significantly relieve the first-cycle irreversible capacity loss, voltage fade and cycling decay [20–22]. A density functional theory calculation suggested that a strong covalent character of the *M*-O bond would likely promote reversible high capacity of Li-rich layered oxides, which can be achieved by substituting *M* (3d) with *M*(4d, 5d) metal cations [23] because *M*(4d, 5d)-O are stronger covalent bonds that enhance the structural stability of Li_2MO_3 and reduce voltage fade during cycling. However, the rate capability of *M*(4d, 5d) substituted Li-rich layered oxides are generally poor (< 50 mAh g^{-1} at 5C) and these materials are more expensive due to the use of noble metals. Thus, simultaneous achieving high discharge capacity, stable voltage during cycling, and low cost remains a major challenge.

In this study, we used a small amount of WO_3 (a 5d transition metal oxide) to "surface dope" a Li-rich layered oxide. WO_3 is selected because it has a low surface free energy and tend to spread spontaneously on the surfaces of other oxides (such as TiO_2 and ZrO_2) during annealing (i.e., segregate or adsorb at the surface thermodynamically that may also change the surface structure and other chemistry, *e.g.*, the critical surface Ni/Mn ratio in this case); such surface phases can form spontaneously as the thermodynamically-preferred surface states via a facile and cost-effective "mixing and annealing" procedure that is employed widely to make so-called "supported oxide catalysts" or "monolayer catalysts" in the petroleum and chemical industries [24–26]. As a result, these WO_3 doped specimens exhibit improved rate capabilities (*e.g.*, retaining a capacity of 90 mAh g^{-1} at a high discharge rate of 40C that represent a 200% improvement from the undoped specimens) and cycling stability as well as reduced voltage fading, in comparison with an undoped benchmark specimen prepared using the identical ball milling and annealing procedure. The improvements are attributed to an appreciable surface chemistry change, *i.e.*, W segregation along with a reversed surface Ni/Mn ratio in comparison with undoped specimen, as revealed by X-ray photoelectron spectroscopy (XPS) in conjunction with ion sputtering, accompanying with simultaneous surface structural disordering and surface valence change, induced by as low as $\sim$1 vol % WO_3 doping.

2. Experimental

The Li-rich prepared by coprecipitation method which is described in our previous publications [4,6]. To prepare 1 vol % WO_3 doped $Li_{1.13}Ni_{0.3}Mn_{0.57}O_2$ (where the volume percentage was calculated based on the molar volumes before mixing and the overall chemical composition is $0.4Li(Li_{1/3}Mn_{2/3})O_2{\cdot}0.6LiMn_{1/2}Ni_{1/2}O_2{\cdot}0.04WO_3$), 0.132 g $(NH_4)_2WO_4$ (Alfa Aesar, 99.99%) precursor (that decomposes to WO_3 upon annealing) was added to 3 g of pristine $Li_{1.13}Ni_{0.3}Mn_{0.57}O_2$ and dispersed in 4 ml of acetone. The mixture was placed in a silicon nitride grinding vial with two silicon nitride balls. High-energy ball milling was carried out using a SPEX 8000D mill for a duration of 10 min, followed by a 15-min resting interval; this milling process was repeated for 3 times. The mixture was dried in an oven isothermally at around 70 °C. The dried powder was placed in a covered alumina crucible, isothermally annealed at 800 °C for 4 h in a box furnace in air with a heating rate of 5 °C/min; subsequently, the specimens were furnace quenched. As a reference, a controlled specimen of undoped $Li_{1.13}Ni_{0.3}Mn_{0.57}O_2$ was prepared with the same ball milling and annealing procedure described above without the addition of the WO_3 precursor.

X-ray diffraction (XRD) was carried out on a diffractometer using Cu K_α radiation (λ = 1.5418 Å) operating at 40 kV and 40 mA with a step size of 0.02° and a step time of 1 s. XRD data analysis was carried out by Rietveld refinement method using FullProf software. Particle sizes and morphologies were characterized using a FEI XL30 scanning electron microscope (SEM).

The surface composition and depth profile of the WO_3 doped $Li_{1.13}Ni_{0.3}Mn_{0.57}O_2$ particles were characterized by XPS. The XPS experiments were carried out by using a Kratos AXIS ULTRA DLD XPS system equipped with an Al Kα monochromated X-ray source and a 165 mm mean radius electron energy hemispherical analyzer. 4 keV Ar ion beam was used for sputtering. The sample current was $\sim$4 μA. Depth profile data were collected after sputtering time of 2 s, 5 s, 10 s, 30 s, and 90 s. The XPS characterization provided the overall surface composition and depth profiles that are averages of many different particles and crystalline facets. All XPS measurements were collected with a 300 mm × 700 mm spot size using a charge neutralizer during acquisition. Survey scans were collected with a 1.0 eV step size, and were followed by high resolution scans with a step size of 0.05 eV for Mn 3p, Ni 2p, and W 4d region. Bonding Energies were calibrated using C 1s peak of 284.6 eV.

Particle surfaces were characterized by high-resolution transmission electron microscopy (HRTEM) using a FEI Titan 80–300 microscope at 300 kV. HRTEM specimens were prepared by dispersing powders ultrasonically in acetone and dropping a small amount of the suspension onto carbon coated copper grids; the specimens were then dried overnight in a desiccator. Minimum exposure was used during HRTEM to reduce electron beam damage.

To prepare cathodes, 80 wt. % active materials, 15 wt. % carbon black (MTI), 5 wt. % PVDF (MTI), and an appropriate amount of NMP (Alfa Aesar, anhydrous, 99.5%) were mixed in a glass vial by a vibrating mixer, followed by ultrasonic dispersion. The mixture was coated on an aluminum foil, which was subsequently dried in a vacuum oven at 90 °C for 6 h. Cathode electrodes with a diameter of 10 mm were punched out, pressed at $\sim$187 MPa, and dried in a vacuum oven at 120 °C for 8 h before transferring into an Ar-filled glovebox for battery construction. The area density of dried electrode coating is $\sim$2.5 mg cm^{-2}. Half cells were made with a cathode electrode, a metal Li chip (MTI, 99.9%) as the anode, 1 M $LiPF_6$ in EC/DMC 1:1 vol electrolyte LP 30, BASF), C480 separator (Celgard), and 2032 coin cell cases (SS304, MTI).

Electrochemical cycling tests were carried out on an Arbin 2143 tester. The rate performance of specimens was tested at the discharge rates of C/20, C/10, C/2, 1C, 2C, 5C, 10C, 20C, 40C, 60C, 80C, 100C, and C/10 sequentially (1C equates to 250 mA h g^{-1}; 1 cycle at each discharge rate) with a constant charge rate of C/10 at room temperature. The cycling stability of $Li_{1.13}Ni_{0.3}Mn_{0.57}O_2$ specimens were measured at a constant charge and discharge rate of 1C between 2.0 V and 4.8 V at room temperature. Electrochemical impedance spectroscopy (EIS) was performed using a Solartron 1287A/1255B analyzer measured from 1 MHz to 0.05 Hz at 10 mV. Cells after the testing were charged to 4.8 V at C/10 and kept for 10 h for subsequent impedance measurements. The EIS data were fitted with the ZView software in the frequency range of 10^5–10 Hz.

3. Results

No obvious difference of particle morphology between undoped and WO_3 doped $Li_{1.13}Ni_{0.3}Mn_{0.57}O_2$ was observed, as shown in Fig. 1. Both specimens have similar agglomerated secondary particles (Fig. 1(a) and (c)). The measured primary particle sizes are 89.8 ± 36.9 nm for the undoped specimen and 88.2 ± 30.5 nm for the WO_3 doped specimen, respectively; the representative SEM images are shown in Fig. 1(b) and (d). The difference in the measured particle sizes is within the range of measurement errors and negligible. Moreover, the primary particles of both undoped and doped specimens have similar round morphology without observed faceting. Hence, a fair comparison study of

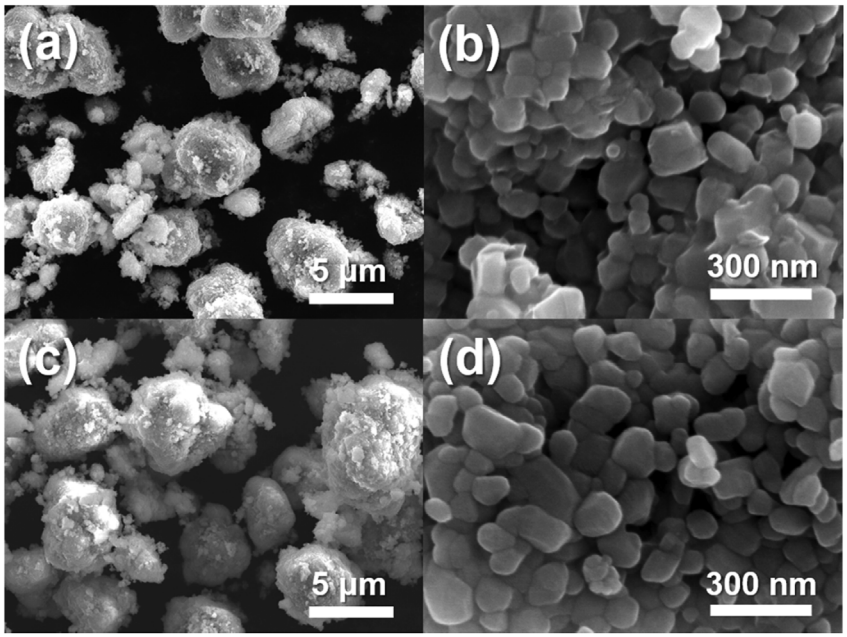

Fig. 1. SEM micrographs of particle morphologies of **(a, b)** undoped and **(c, d)** WO_3 doped $Li_{1.13}Ni_{0.3}Mn_{0.57}O_2$.

electrochemical performance between undoped and doped specimens can be conducted without significant effects of the particle size and morphology.

XRD results reveal only $Li_{1.13}Ni_{0.3}Mn_{0.57}O_2$ peaks in both undoped and WO_3 doped specimens, as shown in Fig. 2. All peaks are indexed to the $R\bar{3}m$ space group that corresponds to the $LiMO_2$ structure, except for the superstructure peaks between 20 and 30° which are associated with a honeycomb ordering of Li, Ni, and Mn in the transition metal layers [9]. The XRD patterns were refined by the Rietveld method. The lattice constants of the undoped $Li_{1.13}Ni_{0.3}Mn_{0.57}O_2$ were obtained as: a = 2.8654(2) and c = 14.257(2) Å), while the WO_3 doped $Li_{1.13}Ni_{0.3}Mn_{0.57}O_2$ has lattice constants of a = 2.8667(2) Å and

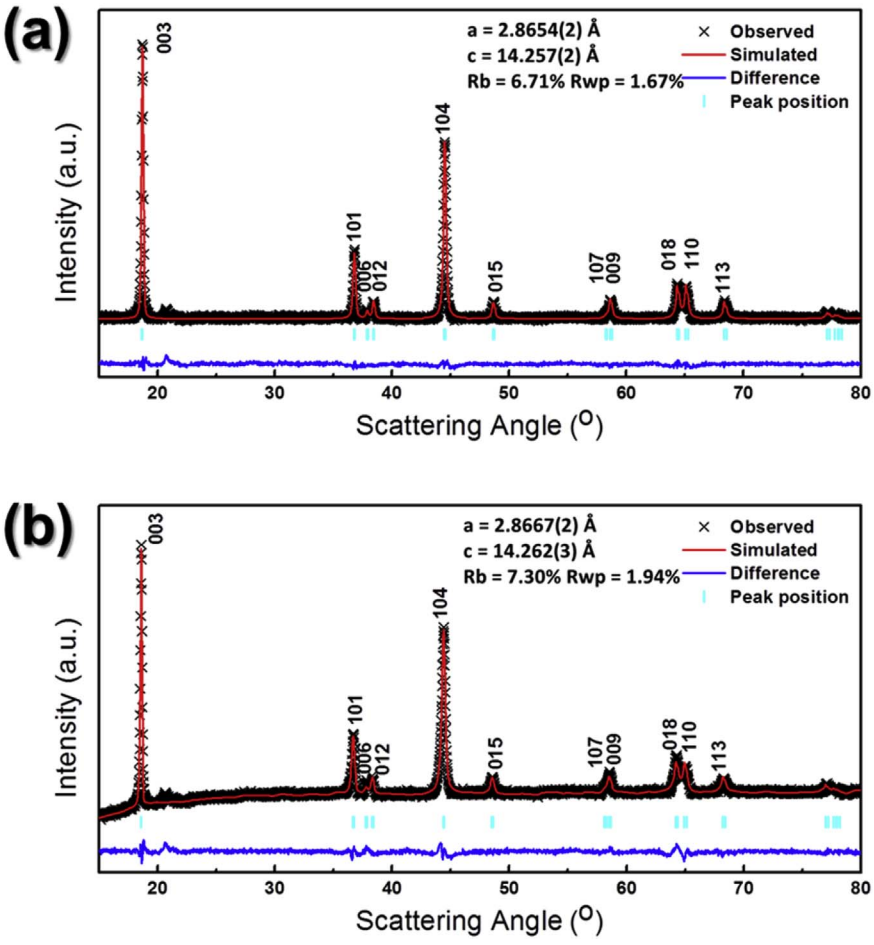

Fig. 2. X-ray diffraction pattern of **(a)** undoped and **(b)** WO_3 doped $Li_{1.13}Ni_{0.3}Mn_{0.57}O_2$. Rietveld refinements have been formed.

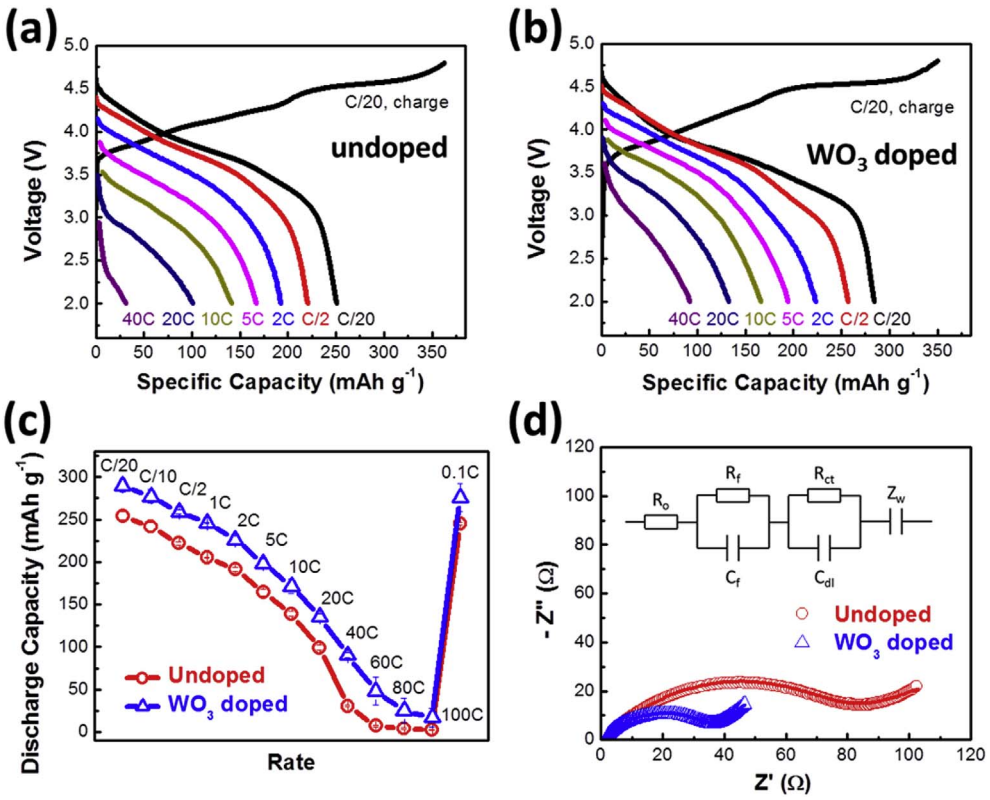

Fig. 3. The rate performance of undoped and doped specimens. Charge/discharge curves of **(a)** undoped and **(b)** WO_3 doped $Li_{1.13}Ni_{0.3}Mn_{0.57}O_2$ at various rates. The black lines represent the initial change/discharge curves tested at C/20 (1C = 250 mAh g^{-1}) and color lines show subsequent discharge curves at various rates labeled in the graph (with a constant charge rate of C/5). **(c)** Rate capabilities of undoped (red circles) and WO_3 doped (blue triangles) $Li_{1.13}Ni_{0.3}Mn_{0.57}O_2$. Three coin cells were made and tested for each specimen. The means are presented and error bars represent ± one standard deviations. **(d)** Electrochemical impedance spectra of undoped (red circles) and WO_3 doped (blue triangles) $Li_{1.13}Ni_{0.3}Mn_{0.57}O_2$. The fittings were based on the equivalent circuit shown in the inset. All tests were performed at room temperature in a voltage window of 2.0–4.8 V. (For interpretation of the references to colour in this figure legend, the reader is referred to the web version of this article.)

c = 14.262(2) Å. The slight increases in the lattice parameters of the WO_3 doped specimen indicates the W is successfully doped into the Li-rich.

A comparison of Fig. 3(a) and Fig. 3(b) shows that the WO_3 doped specimen has a higher initial discharge capacity tested at C/20 and room temperature. On one hand, the first-cycle charge and discharge capacities for the undoped specimen are 363 and 251 mAh g^{-1}, respectively, with a coulombic efficiency of 69%, which are consistent with the typical values reported in prior studies [10,27,28]. On the other hand, the WO_3 doped specimen has charge and discharge capacities of 350 and 284 mAh g^{-1}, respectively, with an improved coulombic efficiency of 81% (representing a 12% increase from that of the undoped specimen). Correspondingly, the reversible discharge capacity is increased by 33 mAh g^{-1} or 13% with as low as 1 vol % WO_3 doping, in comparison with that of the undoped specimen.

The WO_3 doping improves the rate capability significantly. With WO_3 doping, the discharge capacity is increased from 164 to 198 mAh g^{-1} (by ~21%) at 5C, and from 30 to 90 mAh g^{-1} (by ~200%) at 40C on an average as shown in Fig. 3(c). The cells after the rate performance test were characterized by electrochemical impedance spectroscopy (EIS) and the spectra are shown in Fig. 3(d). The EIS results have revealed that the WO_3 doped specimen has smaller total resistance than that of the undoped specimen. After WO_3 doping, the charge transfer resistance decreases from 66.6 Ω to 18.9 Ω, while the surface film resistance in fact increases from 3.5 Ω to 13.3 Ω; thus, the total resistance decreases from 70.1 Ω to 32.2 Ω by 54% with WO_3 doping.

The cycling stability is also enhanced by WO_3 doping, as shown in Fig. 4. The WO_3 doped specimen maintains a discharge capacity of 188 mAh g^{-1} after 100 cycles at a relatively high charge and discharge rate of 1C, which is about 27% higher than that of the undoped specimen (Fig. 4(a)). This improved cycling stability is comparable with some of the best reported performance in literature [12,27]. Furthermore, the voltage fading is also mitigated significantly by minor WO_3 doping, which is in Fig. 4(b). Consequently, an energy density of ~664.6 Wh kg^{-1} is achieved after 100 cycles at 1C, which represents an ~30% improvement from the undoped specimen (Fig. 4(c)).

Figs. 5 and 6 shows XPS results of the undoped and doped specimens. XPS spectra were collected before ion sputtering and after sputtering for 2 s, 5 s, 10 s, 30 s and 90 s. The sputtering rate was calibrated to be about 30 nm per min using a SiO_2 reference specimen sputtered at the same experimental condition [29]. We believe that the W segregation occurs on the surfaces of the primary particles at a thermodynamic equilibrium during the annealing; the secondary particles are essentially agglomeration of the primary particles. The XPS signals were collected from a large area of 300 mm × 700 mm to represent the overall averaged results from many particle surfaces.

The observed W $4d_{5/2}$ peak before sputtering in Fig. 5(a) suggests that most W cations at the surfaces are W^{5+} in doped $Li_{1.13}Ni_{0.3}Mn_{0.57}O_2$ instead of the more stable W^{6+} in WO_3. The binding energies of the W^{6+}, W^{5+}, and W^{4+} cations, respectively, correspond to are 248.2, 245.7 and 243.5 eV, respectively [30]; the brown, blue, and green lines, respectively, are the fitted peaks for the W^{6+}, W^{5+}, and W^{4+} cations, respectively. Specifically, W^{5+} has the highest atomic ratio of 73 ± 7%, in comparison with 16 ± 8% of W^{6+} and 11 ± 3% of W^{4+}. Furthermore, the binding energy of W $4f_{7/2}$ shifts from 35.1 eV to 35.3 eV after sputtering (Fig. 5(b)) [31], which indicates that W valence increases with sputtering time; in other words, W^{6+} cations (representing the most stable valent of W in bulk phase like WO_3) likely dominate in the bulk phase, while W^{5+} cations could dominate at the surfaces. In summary, the majority W cations are reduced from W^{6+} (in the bulk phase) to W^{5+} at the surface.

For both undoped and doped specimens, the binding energy of Mn 3p peak before sputtering is ~49.7 eV, which shifted to ~48.2 eV after sputtering 90 s (Fig. 6(a) and (c)); the decrease of binding energy with the sputtering time represents a decrease of Mn valence, which indicates an increase of Mn^{3+} concentration from surface to bulk, though Mn^{4+} still dominates inside the bulk phase [32,33]. Fig. 6(b) and (d) also show that the binding energy of Ni peaks do not change with sputtering time for both specimens.

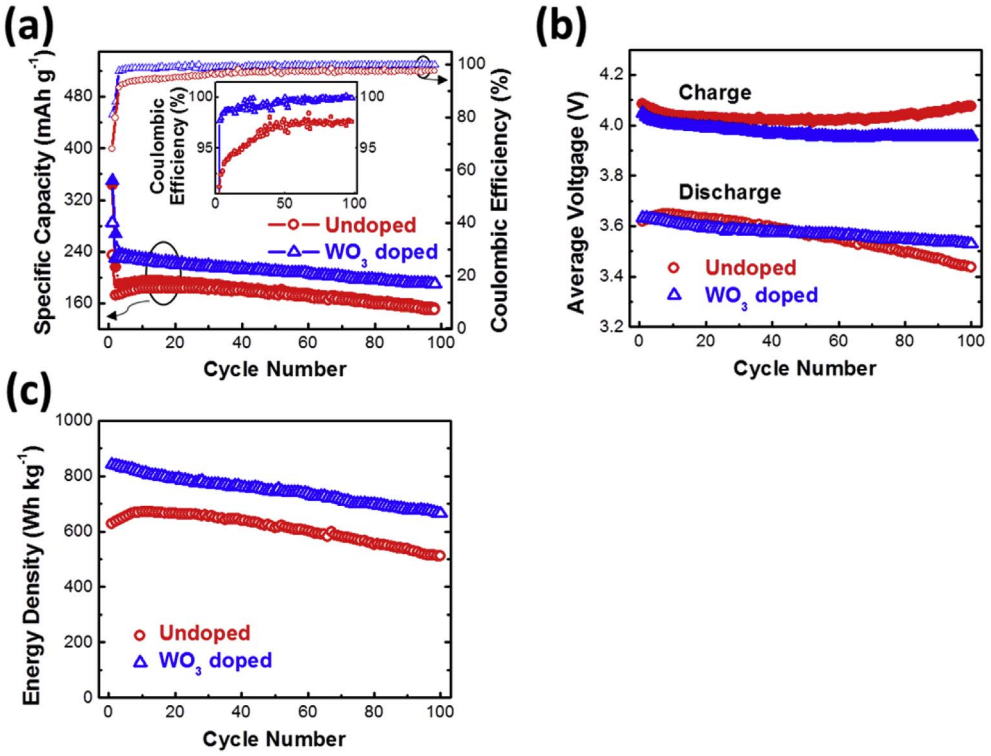

Fig. 4. The cycling performances of undoped (red circles) and WO_3 doped (blue triangles) $Li_{1.13}Ni_{0.3}Mn_{0.57}O_2$ specimens, where the solid and hollow symbols represent charge and discharge performances, respectively. **(a)** The specific capacity *vs.* cycle number curves, where Coulombic efficiencies are also plotted using smaller symbols. Insert is the replotted Coulombic efficiency in a smaller range of 90%–101%. **(b)** Average voltage fading and **(c)** energy density *vs.* cycle number curves. Both undoped and doped specimens were cycled at a charge/discharge rate of 1C at room temperature in the voltage window of 2.0–4.8 V. (For interpretation of the references to colour in this figure legend, the reader is referred to the web version of this article.)

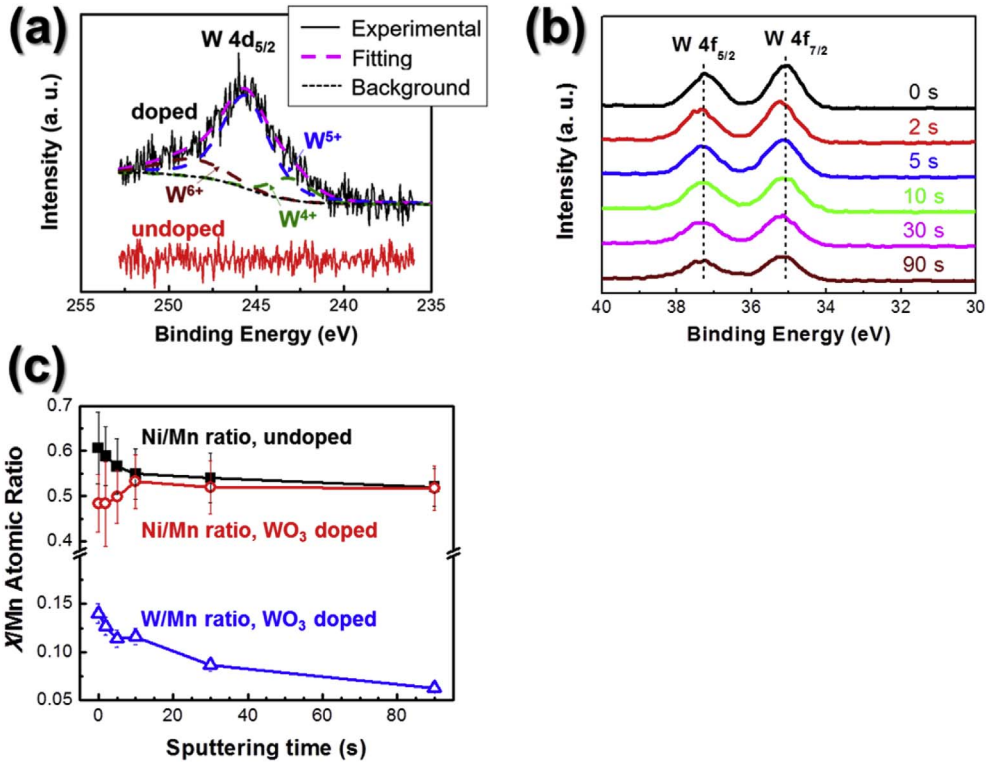

Fig. 5. X-ray photoelectron spectrum of (a) $W4d_{5/2}$ before sputtering and (b) W 4f of doped specimen. (c) Ni/Mn and W/Mn atomic ratios vs. sputtering time for undoped and WO_3 doped $Li_{1.13}Ni_{0.3}Mn_{0.57}O_2$. Noting that the sputtering rate was calibrated to be about 30 nm per min (0.5 nm per second) using a SiO_2 reference specimen sputtered at the same experimental condition.

XPS in conjunction with sputtering also shows the surface segregation (enrichment) of W (Fig. 5(c)), while W is also present inside the bulk phase. Furthermore, the surface segregation of W leads to a decrease of Ni/Mn ratio on the surface; interestingly, the surface of the undoped specimen is enriched with Ni, whereas the surface of the WO_3 doped specimen is enriched of Mn.

This work exemplifies an opportunity to use spontaneously-formed surface phases (with simultaneous and spontaneous changes in surface structure/disorder, composition and valence towards the thermodynamically preferred surface state), along with bulk doping, as facile and scalable method to enhance the electrochemical performance of cathode materials.

4. Discussion

Summarizing the results shown in Fig. 5, we know that (1) Ni

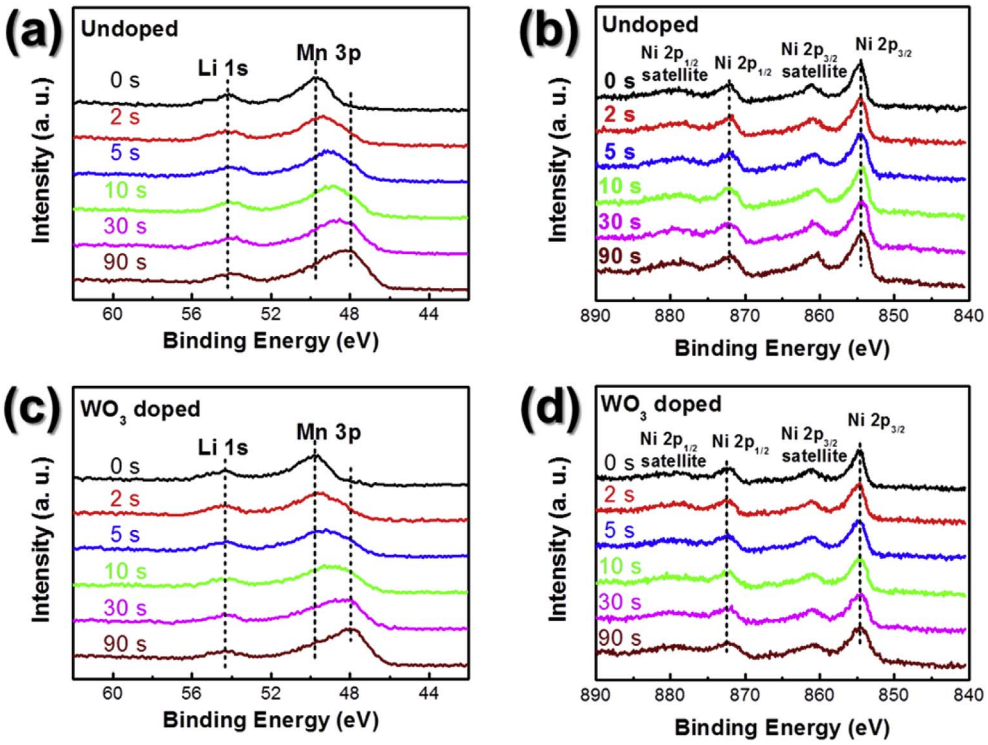

Fig. 6. X-ray photoelectron spectrum of **(a, b)** undoped and **(c, d)** WO_3 doped $Li_{1.13}Ni_{0.3}Mn_{0.57}O_2$, where the binding energies represent **(a, c)** Mn 3p, **(b, d)** Ni 2p.

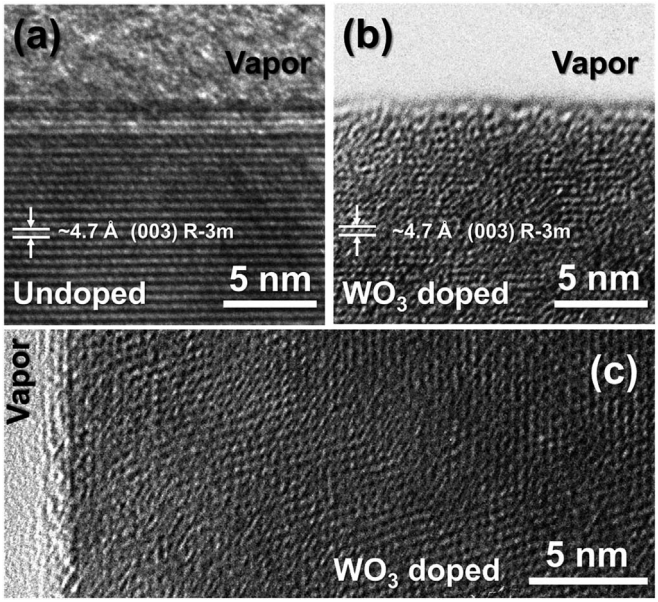

Fig. 7. HRTEM images of **(a)** undoped and **(b, c)** WO_3 doped $Li_{1.13}Ni_{0.3}Mn_{0.57}O_2$. Both undoped and doped specimens were fabricated via an identical procedure by ball milling and subsequently annealed at 800 °C for 4 h. The "vapor" shown in the pictures means that the specimen was exposed in a vacuum environment during the observation. The region above specimen in Fig. 7(a) was amorphous carbon on the grid since the sample was prepared on a copper grid with carbon film coating.

segregates at the surfaces in the undoped specimen; (2) W segregates at the surfaces with a surface reduction (W^{6+} inside the bulk phase *vs.* predominately W^{5+} at the surface), and (3) the surface segregation of W suppresses the surface segregation of Ni to increase (reverse) the relative surface Ni/Mn ratio (w.r.t. that in the bulk phase) in comparison with the undoped surface (Fig. 5(c) noting the absolute surface Mn cation ratio may not increase because of surface enrichment of W). Furthermore, HRTEM images (Fig. 7) show that the surfaces of WO_3 doped specimen is more disordered than that of the undoped specimen. Noting that we carefully monitored the change of surfaces during the HRTEM imaging and we did not observe the any amorphization or other significant damages during the observation so that the disordering was not caused by the beam irradiation under HRTEM.

Such a unique surface configuration in the WO_3 doped $Li_{1.13}Ni_{0.3}Mn_{0.57}O_2$ formed spontaneously (during annealing) as the equilibrium surface thermodynamic state with its own thermodynamically-determined chemistry (composition and valence states; Fig. 5) and structure (more disordered; Fig. 7) that are markedly different from those of the underneath bulk phase. Thus, the thermodynamically-determined surface state can be considered as a 2-D surface phase (also called "complexion" to differentiate it from a thin surface layer/coating of a bulk phase [19,34,35]), akin to those nanoscale surface amorphous films (SAFs) [18,36–38] and other surface complexions [39] previously observed to form in a few other battery materials that improved the rate capabilities [18,36,38–40] and cycling stabilities [18]. In contrast to the prior cases of phosphate-based, nanometer-thick SAFs that are discrete in HRTEM, the 2-D surface phase observed in the WO_3 doped $Li_{1.13}Ni_{0.3}Mn_{0.57}O_2$ appears to have more gradually-varying profiles of composition and structures (Figs. 3 and 4). Nonetheless, this surface phase observed in the WO_3 doped $Li_{1.13}Ni_{0.3}Mn_{0.57}O_2$ in this study can also contribute to improved rate capability and cycling stability as well as reduced charge transfer and voltage fading (similar to other types of surface phases [18,36,38–40]). Specifically, several possible benefits of this surface phase can be discussed.

In the first charge, the region below ~4.4 V is usually attributed to a reversible Ni^{2+}/Ni^{4+} oxidation, corresponding to the lithium extraction from the lithium layer [5]. The plateau above 4.4 V is attributed to a partially reversible anionic O^{2-}/O^{2-x} and irreversible oxygen loss, corresponding to the lithium extraction from the lithium layer and transition metal layer with oxygen vacancy formation, which will inevitably lead to the migration of transition metal cations from the transition metal layer to the lithium layer [3,12,41]. Consequently, there is always a high irreversible capacity observed in the first cycle of Li-rich. A prior study showed that in the $Li_2Ru_xMn_{1-x}O_3$ with Ru partial substitution of Mn, a Ru^{5+}/Ru^{4+} redox was accompanied by the $O^{2-}/$

O^- redox processes [22]. It is also suggested that *M*(4d, 5d)-O bonds are stronger than those of *M*(3*d*)-O and can enhance the M-O covalency and structural stability of Li_2MO_3 [23]. Likewise, W doping in $Li_{1.13}Ni_{0.3}Mn_{0.57}O_2$ phase (as well as the spontaneous formation of WO_3 segregation induced surface phase) may also have similar stabilization effects as those of Ru. Specifically, W has a higher formation enthalpy of W-O (~598–632 kJ mol^{-1}) than that of Mn-O (~402 kJ mol^{-1}) and Ni-O (391.6 kJ mol^{-1}), which may strengthen the M-O covalency and reduce oxygen release from breaking M-O bonds (via promoting reversible $M\text{-}O^{2-}/M\text{-}O^{2-x}$ redox instead of oxygen loss from lattice structure) [20]. In this work, the first cycle irreversible capacity of Li-rich is significantly reduced from 112 mAh g^{-1} to 66 mAh g^{-1} by W doping. At the same time, the reversible discharge capacity of W doped specimen shows 33 mAh g^{-1} enhancement than the undoped specimen. All these facts suggest that the W doping may suppress the irreversible oxygen loss and facilitate the reversible O^{2-}/O^- redox processes, which could help to maintain the structural stability of Li-rich and further improve the cycling performance.

The low oxidation state cation (Ni^{2+}) migration to the lithium layer blocks the lithium diffusion during electrochemical charge and discharge, which leads to poor rate capability. The existence of oxygen vacancy facilitates this cation migration [7]. In this work, it appears that WO_3 doping and surface segregation decreases the Ni content at the surface. As a consequence, the transition metal migration might be suppressed, results in an improved rate performance of Li-rich [3].

5. Conclusions

As low as 1 vol % WO_3 doping can simultaneously enhance the reversible capacity in the first cycle, the rate capability, and the cycling stability, as well as reduce voltage fading, of the $Li_{1.13}Ni_{0.3}Mn_{0.57}O_2$ cathode material. XPS (with depth profiling) and HRTEM characterizations showed that W segregates at the particle surfaces, occurring concurrently with a surface reduction of W, a change of surface Ni/Mn ratio, and surface structural disordering. Consequently, a thermodynamically-preferred surface structure forms spontaneously, which can be considered as a surface phase or complexion. The spontaneous formation of this surface phase benefits both cycling stability and rate capability. It is further suggested that the stronger covalent character of the W-O bond could alleviate oxygen loss on the surface and the migration of the transition metal cations.

This work suggests, and subsequently exemplifies, a new strategy of improving the performance of Li-rich layered oxide and potentially other cathode and anode materials via a facile and cost-effective “mixing and annealing” procedure to enable their uses in the next-generation batteries thru the spontaneous formation of thermodynamically-preferred surface phases.

Acknowledgements

This work was primarily supported by a Vannevar Bush Faculty Fellowship sponsored by the Basic Research Office of the Assistant Secretary of Defense for Research and Engineering and funded by the Office of Naval Research through grant N00014-16-1-2569. J. Huang would like to thank Dr. Ich Tran for his help with the XPS experiments at the University of California, Irvine Materials Research Institute (IMRI) using instrumentation funded in part by the National Science Foundation Major Research Instrumentation Program under grant no. CHE-1338173. H.D. Liu and Y.S. Meng would acknowledge the partial support from the Assistant Secretary for Energy Efficiency and Renewable Energy, Office of Vehicle Technologies of the U.S. Department of Energy (DOE) under Contract No. DE-AC02-05CH11231, Subcontract No. 7073923, under the Advanced Battery Materials Research (BMR) Program.

References

[1] E.M. Erickson, F. Schipper, T.R. Penki, J.-Y. Shin, C. Erk, F.-F. Chesneau, B. Markovsky, D. Aurbach, Review—recent advances and remaining challenges for lithium ion battery cathodes: II. Lithium-rich, xLi2MnO3·(1-x)LiNiaCobMncO2, J. Electrochem. Soc. 164 (2017) A6341–A6348.
[2] M.M. Thackeray, S.-H. Kang, C.S. Johnson, J.T. Vaughey, R. Benedek, S.A. Hackney, Li2MnO3-stabilized LiMO2 (M = Mn, Ni, Co) electrodes for lithium-ion batteries, J. Mat. Chem. 17 (2007) 3112–3125.
[3] S. Hy, H.D. Liu, M.H. Zhang, D.N. Qian, B.J. Hwang, Y.S. Meng, Performance and design considerations for lithium excess layered oxide positive electrode materials for lithium ion batteries, Energ Environ. Sci. 9 (2016) 1931–1954.
[4] M.G. Verde, H.D. Liu, K.J. Carroll, L. Baggetto, G.M. Veith, Y.S. Meng, Effect of morphology and manganese valence on the voltage fade and capacity retention of Li [Li2/12Ni3/12Mn7/12]O-2, Acs Appl. Mater Inter 6 (2014) 18868–18877.
[5] H.D. Liu, Y. Chen, S. Hy, K. An, S. Venkatachalam, D.N. Qian, M.H. Zhang, Y.S. Meng, Operando lithium dynamics in the Li-Rich layered oxide cathode material via neutron diffraction, Adv. Energy Mater 6 (2016).
[6] H.D. Liu, C.R. Fell, K. An, L. Cai, Y.S. Meng, In-situ neutron diffraction study of the xLi(2)MnO(3)center dot(1-x)LiMO2 (x=0, 0.5; M = Ni, Mn, Co) layered oxide compounds during electrochemical cycling, J. Power Sources 240 (2013) 772–778.
[7] D. Qian, B. Xu, M. Chi, Y.S. Meng, Uncovering the roles of oxygen vacancies in cation migration in lithium excess layered oxides, PCCP 16 (2014) 14665–14668.
[8] P. Yan, L. Xiao, J. Zheng, Y. Zhou, Y. He, X. Zu, S.X. Mao, J. Xiao, F. Gao, J.-G. Zhang, C.-M. Wang, Probing the degradation mechanism of Li2MnO3 cathode for Li-Ion batteries, Chem. Mater 27 (2015) 975–982.
[9] B. Xu, C.R. Fell, M. Chi, Y.S. Meng, Identifying surface structural changes in layered Li-excess nickel manganese oxides in high voltage lithium ion batteries: a joint experimental and theoretical study, Energ Environ. Sci. 4 (2011) 2223–2233.
[10] A.R. Armstrong, M. Holzapfel, P. Novák, C.S. Johnson, S.-H. Kang, M.M. Thackeray, P.G. Bruce, Demonstrating oxygen loss and associated structural reorganization in the lithium battery cathode Li[Ni0.2Li0.2Mn0.6]O2, J. Am. Chem. Soc. 128 (2006) 8694–8698.
[11] A. Boulineau, L. Simonin, J.-F. Colin, C. Bourbon, S. Patoux, First evidence of manganese–nickel segregation and densification upon cycling in Li-Rich layered oxides for lithium batteries, Nano Lett. 13 (2013) 3857–3863.
[12] X. Yu, Y. Lyu, L. Gu, H. Wu, S.-M. Bak, Y. Zhou, K. Amine, S.N. Ehrlich, H. Li, K.-W. Nam, X.-Q. Yang, Understanding the rate capability of high-energy-density Li-Rich layered Li1.2Ni0.15Co0.1Mn0.55O2 cathode materials, Adv. Energy Mater. 4 (2014) 1300950.
[13] J. He, X. Chu, Y.-B. He, D. Liu, Y. Liu, J. Wu, B. Li, F. Fang, Li2SiO3 coating to improve the high-voltage performance of LiNi1/3Co1/3Mn1/3O2 cathode, Int. J. Electrochem. Sci. 11 (2016) 6902–6913.
[14] X. He, J. Wang, B. Qiu, E. Paillard, C. Ma, X. Cao, H. Liu, M.C. Stan, H. Liu, T. Gallash, Y.S. Meng, J. Li, Durable high-rate capability Na0.44MnO2 cathode material for sodium-ion batteries, Nano Energy 27 (2016) 602–610.
[15] Y. Liu, K. Qian, J. He, X. Chu, Y.-B. He, M. Wu, B. Li, F. Kang, In-situ polymerized lithium polyacrylate (PAALi) as dual-functional lithium source for high-performance layered oxide cathodes, Electrochim. Acta 249 (2017) 43–51.
[16] N.M. Trease, I.D. Seymour, M.D. Radin, H. Liu, H. Liu, S. Hy, N. Chernova, P. Parikh, A. Devaraj, K.M. Wiaderek, P.J. Chupas, K.W. Chapman, M.S. Whittingham, Y.S. Meng, A. Van der Van, C.P. Grey, Identifying the distribution of Al3+ in LiNi0.8Co0.15Al0.05O2, Chem. Mater 28 (2016) 8170–8180.
[17] D. Xu, Y.-B. He, X. Chu, Z. Ding, B. Li, J. He, H. Du, X. Qin, F. Kang, Synthesis of lithium iron phosphate/carbon microspheres by using polyacrylic acid coated iron phosphate nanoparticles derived from iron(III) acrylate, ChemSusChem 8 (2015) 1009–1016.
[18] J. Huang, J. Luo, A facile and generic method to improve cathode materials for lithium-ion batteries via utilizing nanoscale surface amorphous films of self-regulating thickness, Phys. Chem. Chem. Phys. 16 (2014) 7786–7798.
[19] P.R. Cantwell, M. Tang, S.J. Dillon, J. Luo, G.S. Rohrer, M.P. Harmer, Overview No. 152: grain boundary complexions, Acta Mater. 62 (2014) 1–48.
[20] M. Sathiya, G. Rousse, K. Ramesha, C.P. Laisa, H. Vezin, M.T. Sougrati, M.L. Doublet, D. Foix, D. Gonbeau, W. Walker, A.S. Prakash, M. Ben Hassine, L. Dupont, J.M. Tarascon, Reversible anionic redox chemistry in high-capacity layered-oxide electrodes, Nat. Mater 12 (2013) 827–835.
[21] M. Sathiya, A.M. Abakumov, D. Foix, G. Rousse, K. Ramesha, M. Saubanère, M.L. Doublet, H. Vezin, C.P. Laisa, A.S. Prakash, D. Gonbeau, G. VanTendeloo, J.M. Tarascon, Origin of voltage decay in high-capacity layered oxide electrodes, Nat. Mater 14 (2015) 230–238.
[22] M. Sathiya, K. Ramesha, G. Rousse, D. Foix, D. Gonbeau, A.S. Prakash, M.L. Doublet, K. Hemalatha, J.M. Tarascon, High performance Li2Ru1–yMnyO3 ($0.2 \le y \le 0.8$) cathode materials for rechargeable lithium-ion batteries: their understanding, Chem. Mater 25 (2013) 1121–1131.
[23] Y. Xie, M. Saubanere, M.L. Doublet, Requirements for reversible extra-capacity in Li-rich layered oxides for Li-ion batteries, Energ Environ. Sci. 10 (2017) 266–274.
[24] J. Luo, Y.M. Chiang, Existence and stability of nanometer-thick disordered films on oxide surfaces, Acta Mater 48 (2000) 4501–4515.
[25] M. Scheithauer, R.K. Grasselli, H. Knözinger, Genesis and structure of WOx/ZrO2 solid acid catalysts, Langmuir 14 (1998) 3019–3029.
[26] Y. Tae Kwon, K. Yong Song, W. In Lee, G. Jin Choi, Y. Rag Do, Photocatalytic behavior of WO3-loaded TiO2 in an oxidation reaction, J. Catal. 191 (2000) 192–199.
[27] D. Wang, I. Belharouak, G. Zhou, K. Amine, Nanoarchitecture multi-structural cathode materials for high capacity lithium batteries, Adv. Funct. Mater 23 (2013)

1070–1075.
[28] A. Manthiram, Y. Fu, S.-H. Chung, C. Zu, Y.-S. Su, Rechargeable lithium–sulfur batteries, Chem. Rev. 114 (2014) 11751–11787.
[29] J. Liu, A. Manthiram, Understanding the improved electrochemical performances of Fe-Substituted 5 V spinel cathode LiMn1.5Ni0.5O4, J. Phys. Chem. C 113 (2009) 15073–15079.
[30] A. Romanyuk, R. Steiner, L. Marot, P. Oelhafen, Temperature-induced metal–semiconductor transition in W-doped VO2 films studied by photoelectron spectroscopy, Sol. Energy Mater. Sol. Cells 91 (2007) 1831–1835.
[31] S.F. Ho, S. Contarini, J.W. Rabalais, Ion-beam-induced chemical changes in the oxyanions (Moyn-) and oxides (Mox) where M = chromium, molybdenum, tungsten, vanadium, niobium and tantalum, J. Phys. Chem. 91 (1987) 4779–4788.
[32] L. Baggetto, N.J. Dudney, G.M. Veith, Surface chemistry of metal oxide coated lithium manganese nickel oxide thin film cathodes studied by XPS, Electrochimica Acta 90 (2013) 135–147.
[33] H. Liu, D. Qian, M.G. Verde, M. Zhang, L. Baggetto, K. An, Y. Chen, K.J. Carroll, D. Lau, M. Chi, G.M. Veith, Y.S. Meng, Understanding the role of NH4F and Al2O3 surface Co-modification on lithium-excess layered oxide Li1.2Ni0.2Mn0.6O2, ACS Appl. Mat. Interfaces 7 (2015) 19189–19200.
[34] W.D. Kaplan, D. Chatain, P. Wynblatt, W.C. Carter, A review of wetting versus adsorption, complexions, and related phenomena: the rosetta stone of wetting, J. Mater. Sci. 48 (2013) 5681–5717.
[35] J. Luo, Interfacial engineering of solid electrolytes, J. Materiomics 1 (2015) 22–32.
[36] A. Kayyar, H.J. Qian, J. Luo, Surface adsorption and disordering in LiFePO4 based battery cathodes, Appl. Phys. Lett. 95 (2009) 221905.
[37] J. Luo, Y.-M. Chiang, Wetting and prewetting on ceramic surfaces, Annu. Rev. Mater. Res. 38 (2008) 227–249.
[38] B. Kang, G. Ceder, Battery materials for ultrafast charging and discharging, Nature 458 (2009) 190–193.
[39] M. Samiee, J. Luo, A facile nitridation method to improve the rate capability of TiO2 for lithium-ion batteries, J. Power Sources 245 (2014) 594–598.
[40] D. Geng, N. Ding, T.S.A. Hor, S.W. Chien, Z. Liu, D. Wuu, X. Sun, Y. Zong, From lithium-oxygen to lithium-air batteries: challenges and opportunities, Adv. Energy Mater. 6 (2016) (n/a-n/a).
[41] D. Mohanty, S. Kalnaus, R.A. Meisner, A.S. Safat, J. Li, E.A. Payzant, K. Rhodes, I.I.I.D.L. Wood, C. Daniel, Structural transformation in a Li1.2Co0.1Mn0.55Ni0.15O2 lithium-ion battery cathode during high-voltage hold, RSC Adv. 3 (2013) 7479–7485.